Int J Adv Manuf Technol (2009) 42:421–428
DOI 10.1007/s00170-008-1620-4

ORIGINAL ARTICLE

A coupled thermal–mechanical analysis of a mold-billet system during continuous casting

J. Zhou · X. Peng · Y. Qin

Received: 14 March 2008 / Accepted: 16 June 2008 / Published online: 12 July 2008

Abstract The three-dimensional (3-D) thermal–mechanical behavior of a mold–billet system under actual casting conditions is investigated with an finite element approach, taking into account the main influencing factors, such as solidification heat, latent heat released during phase transformation, heat transfer, as well as the interaction between the moving billet and the mold. It is based on the coupled thermal–mechanical analysis for the whole mold–billet system, instead of analyzing the thermal–mechanical behavior of the mold and the billet individually, as is often used in practice. Comparison shows that the former approach can provide satisfactory results without making use of the empirical estimation of the heat flux through the inboard surface of the mold based on the difference between the temperature of inlet and outlet cooling water at steady-state and the temperature distribution near the surface of the inboard plate measured experimentally, which are usually necessarily required for the latter approach to be applied in practice.

Keywords Continuous casting · Mold–billet system · Coupled thermal–mechanical analysis · FE simulation

J. Zhou (✉) · X. Peng
Department of Engineering Mechanics, Chongqing University,
Chongqing 400044, China
e-mail: zhoujiayong1976@163.com

Y. Qin (✉)
Department of Design, Manufacture and Engineering
Management, University of Strathclyde,
Glasgow G1 1XJ, UK
e-mail: qin.yi@strath.ac.uk

1 Introduction

Continuous casting has been employed widely in steel industry due to its inherent advantages of low cost, high productivity, flexibility of operation, and the capability of achieving high quality of products. In a continuous casting process, as shown in Fig. 1, molten steel flows from a ladle, through a tundish into a "semifinished shape" slab, bloom, or billet for subsequent rolling in the finishing mills. Continuous casting represents a tremendous savings in time, labor, energy, and capital. By casting the steel directly into semifinished shapes, the following steps are eliminated: ingot teeming, stripping, and transfer, soaking pits, and primary rolling [1–4].

Heat transfer plays a critical role during a continuous casting process, which determines significantly the productivity and quality of the cast products [5–8]. The mold extracts the solidification heat from the billet and transfers the heat to the cooling water, supports the liquid steel, and makes the billet solidify and form a sufficiently thick solid shell, which is necessary to prevent the breakout of liquid steel.

A correct estimation of the distribution of the temperature in the billet can help in predicting the thickness of the solid steel shell [9–12] and is necessary for the control of production and the optimization of technology. Although great efforts and progress have been made in the investigation of continuous casting processes, less effort has been made in coupled thermal–mechanical analysis of the whole mold–billet system.

It is known that the interaction between the mold and the moving billet is important for the productivity and the quality of the products, but such coupling is usually incompletely taken into account as the behavior of the mold, and the billet is investigated individually. For

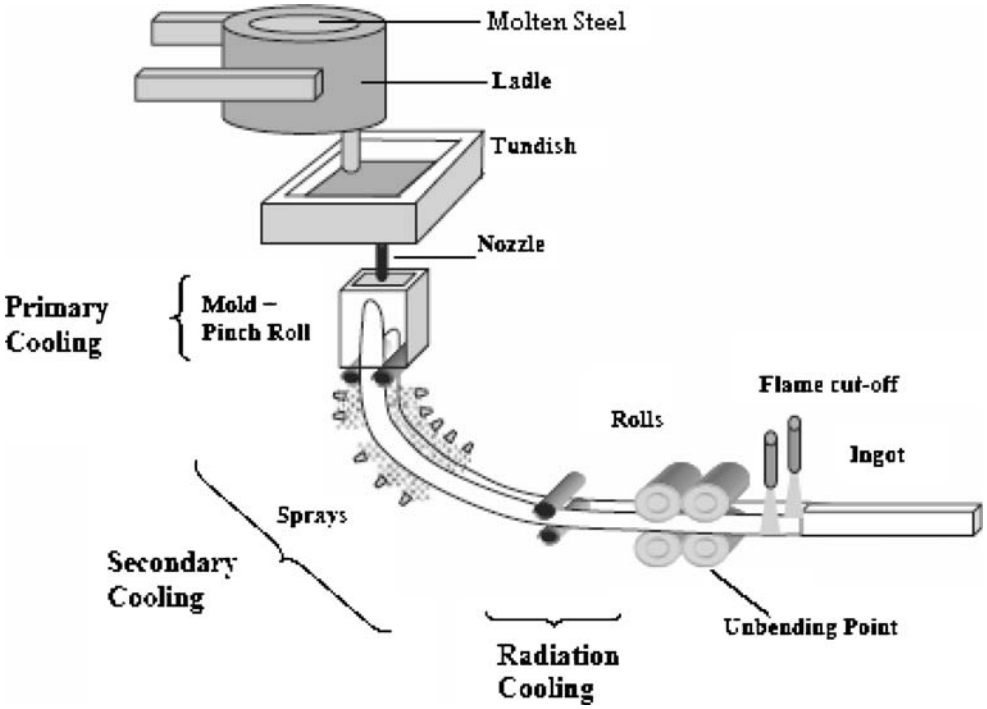

Fig. 1 The typical Schematic representation of the continuous casting process

example, when investigating the behavior of the mold, the mechanical interaction between the billet and the mold is seldom considered. While, the thermal interaction, i.e., the heat exchange between the mold and the billet, is usually estimated with empirical methods.

The steady-state distributions of the temperature in continuous casting molds and the optimization of the cooling water slot system were investigated by the authors recently [11], in which the thermal response of the mold was analyzed individually, and the thermal interaction between the billet and the mold was considered as the heat flux through the inboard surface of the mold, which was determined empirically and experimentally. Although this kind of approach is currently used in practice, the following problems remain unsolved: (a) the empirical formulae of the heat flux identified with specific experiment lack generality; (b) splitting a mold–billet system into two individual parts may not only ignore the interaction between them and lead to inconsistency but also add difficulty and complexity to the analysis; and (c) the corresponding approach may exclude the mechanical interaction between the mold and the billet, therefore it cannot provide available information for a correct prediction of the possible wear and failure of the mold.

In this paper, finite element (FE) simulation of the coupled thermal–mechanical behavior of a mold–billet system during continuous casting is reported. It takes into account solidification heat, latent heat released during phase transformation, heat transfer, and the interaction between the moving billet and the copper plate of the mold, as well as their effects on the subsequent casting processes. It can be seen that with the solidification of the billet, a large quantity of the heat is transferred from the liquid steel to the cooling water through the mold and that the solid steel shell is formed while the billet moves downwards. The temperature distribution in the mold depends strongly on the properties of both the mold–billet system and the cooling water system. For comparison, the mold–billet system with the same material and structural parameters, as shown in [11], is also analyzed. The comparison shows that, although the results being compared are similar to each other, the coupled thermal–mechanical approach for the whole mold–billet system is able to provide more comprehensive and realistic results with fewer assumptions and empirical means, and it will be more powerful for practical applications.

2 FE modeling of a mold–billet system

2.1 The parameters of the mold–billet system

The parameters of the mold and the continuous casting considered are shown in Table 1. The configuration of the mold–billet system at the end of the computation is shown in Fig. 2. At the start of the computation, the bottom of the molten billet is located at h=0, i.e., the top of the mold (Fig. 2). The temperature of the cooling water is assumed to

Table 1 Mold parameters and continuous casting conditions

Parameters/conditions		
Mold dimensions	1.75×0.17×0.84 m	
Copper plates	Main plate	Side plate
Space between screws (mm)	135	80
The length of slots (mm)	780	780
Space between slots (mm)	24	20
The number of slots	55	7
The sizes of the cross-sections of slots (mm^2)	6×20	5.5×20
Billet dimensions	2×1.7×0.17 m	
Casting velocity	1.2 m/min (0.02 m/s)	
Cooling water flow	48.6 kg/s	
Poured temperature	1,530°C	
Import temperature of cooling water	30°C	
Export temperature of cooling water	38°C	

Table 2 Thermal and mechanical parameters of steel Q235

Parameter	Value
Liquidus temperature T_L (°C)	1,522
Solidus temperature T_S (°C)	1,490
Viscosity of molten steel, μ_l (kg/(m s))	6.2×10^{-3}
Liquid phase density ρ_L (kg/m^3)	$6{,}832+0.279T-9.7\times10^{-5}T^{2a}$
Solid phase density ρ_S (kg/m^3)	$7{,}138+0.21T-6.89\times10^{-5}T^2-3.4\times10^{-9}T^3$
Specific heat c_P [J/(kg °C)]	680
Heat transfer coefficient of solid phase λ_S [W/(m °C)]	$19.16+9.6\times10^{-3}T$
Heat transfer coefficient of liquid phase λ_L [W/(m °C)]	26
Latent heat of H_f (kJ/kg)	284.5
Thermal expansion coefficient, α_S (1/°C)	10^{-4}

T Current temperature(°C)

vary linearly from the inlet to the outlet. In order to avoid the breakage of the solidified shell, a sufficient thickness of the solidified steel shell is necessary to support the liquid steel when the billet moves out of the mold. The investigation to the temperature distribution can provide the information for the improvement of the design and for the control of the casting process. An efficient transfer of the heat from the billet to the mold can also be of help for the improvement of the quality and productivity of the products.

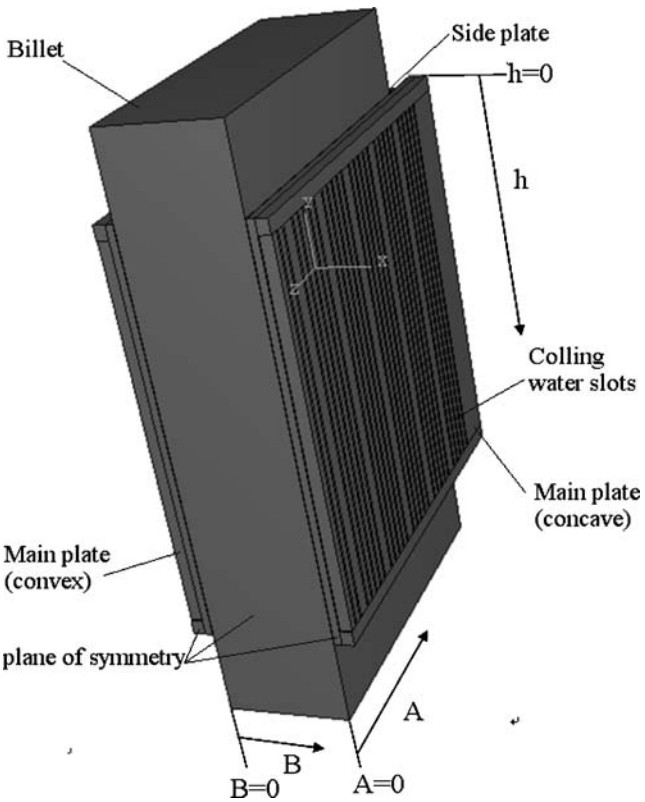

Fig. 2 The mold–billet system for analysis

2.2 Thermal and mechanical properties of the billet and the mold materials [11]

The billet material is Q235, a Fe–0.13% C low-carbon steel, with the main thermal and mechanical properties listed in Table 2.

The mold was made of a Cr–Zr–Cu copper alloy. The mass fractions of the three components are Cr=0.5–1.5%, Zr=0.05–0.3%, and Cu=98%. It possesses excellent heat conductivity and resistance to both wear and corrosion. The corresponding thermal and mechanical parameters are listed in Table 3.

The variation of the yield strength of the copper plate of the mold σ_{SM} with temperature is shown in Fig. 3. It can be seen that although σ_{SM} decreases gradually with the

Table 3 Thermal and mechanical properties of the mold material

Property	Value
Heat transfer coefficient, λ_M [W/(m °C)]	$316.5+0.1263T-1.3905\times10^{-4}T^2$
Density, ρ_M (kg/m^3)	$8{,}920-0.1T-0.00063T^2$
Specific heat, c_{PM} [J/(kg °C)]	$386+0.1T$
Softening temperature, T_{SM} (°C)	500
Thermal expansion coefficient, α_M (1/°C)	1.7×10^{-5}
Young's modulus, E_M (GPa)	120
Poisson's ratio, υ_M	0.27

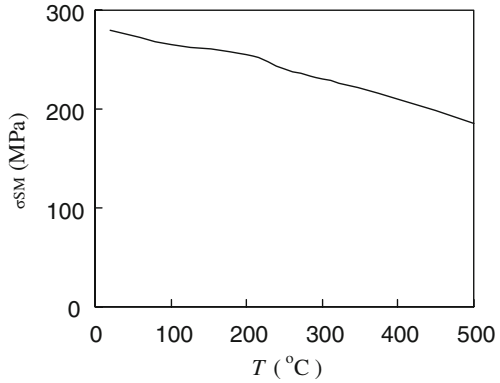

Fig. 3 The variation of the yield strength of the mold material with temperature

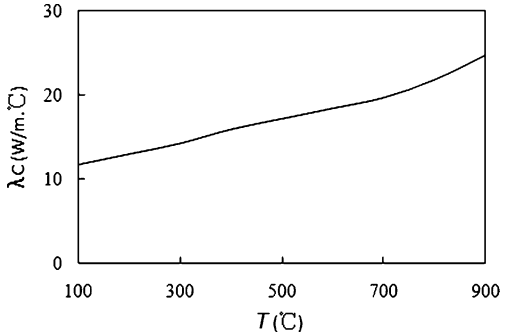

Fig. 4 The variation of the thermal conductivity of the coating against temperature

increase in temperature, it remains sufficiently high if the temperature is below 500°C.

In order to increase the hardness and the resistance against wear, a Ni–Fe coating is plated onto the working surfaces of the mold. It should be noted that at the upper part of the mold, what should be mainly considered is heat conductivity, because in this region, the steel is almost at a molten state so that wear is less significant. While, at the lower part of the mold a solid steel shell has been formed, which is harder and requires the mold to have sufficient resistance against wear. In order to meet these requirements, the thickness of the coating material varies gradually from about 0.5 mm at the top of the working section of the mold to about 1.5 mm at the bottom of the working section of the mold. Such a coating may reduce approximately the heat conductivity to about 4.5% at the top of the working section of the mold and about 17% at the bottom of the working section of the mold [11]. The corresponding thermal and mechanical parameters are listed in Table 4.

The variation of the thermal conductivity of the coating material with temperature is shown in Fig. 4.

Table 4 Thermal and mechanical properties of the coating material

Property	Value
Specific heat, c_{PC} [J/(kg °C)]	565+0.127T
Density, ρ_C (kg/m^3)	7958−0.439T
Thermal expansion coefficient, α_C (1/°C)	1.56×10^{-5}
Young's modulus, E_C (GPa)	153 (20–500°C)
Poisson's ratio, ν_C	0.25
Yield strength, σ_{SC} (MPa)	450 (20–700°C)

3 Governing equation of heat conduction with latent heat

The three-dimensional transient heat conduction energy balance equation for isotropic material can be expressed as [3, 5, 13–16]:

$$\int_V \rho \frac{\mathrm{d}U}{\mathrm{d}t}\mathrm{d}V = \int_S q\mathrm{d}S + \int_V r\mathrm{d}V \tag{1a}$$

or:

$$\rho c\frac{\partial T}{\partial t} - \nabla\cdot(k\nabla T) - \rho Q = 0, \tag{1b}$$

where V is a volume of material (m^3), with surface area S (m^2), ρ is the density of the material (kg/m^3), $\dot{U}$ is the material time rate of the internal energy, q is the heat flux per unit area of the body, flowing into the body, and r is the heat supplied externally into the body per unit volume (W/m^3), Q is the internal strength of heat source (W/kg), with initial condition $T|_{t=0} = T_0$, where T is the temperature (°C), t is time (s), x, y, z are the rectangular coordinates (m), c is the specific heat (J/(kg °C)), and k is the thermal conductivity (W/(m °C)).

4 Initial and boundary conditions

(a) Half of the mold–billet system is used for analysis because of symmetry (Fig. 2). The temperature boundary conditions can be prescribed as

$$T = \overline{T} \text{ on } \Gamma_1, \tag{2}$$

where Γ_1 is the mold surfaces contacting the cooling water tank. Noticing that the difference of the temperatures measured at both sides of the interface is negligible due to very good contact, $\overline{T}$ can be regarded as constant.

(b) The heat-flux boundary condition may be expressed as:

$$k\frac{\partial T}{\partial n} = h(T_\alpha - T) \text{ on } \Gamma_3, \tag{3}$$

where $\frac{\partial T}{\partial n} = \frac{\partial T}{\partial x}n_x + \frac{\partial T}{\partial y}n_y + \frac{\partial T}{\partial z}n_z$ is normal differentiation, h (W/(m^2 °C)) is the convection exchange coefficient, and T_a is the ambient temperature. In simulation, Γ_3 includes the boundaries of the mold contacting cooling water, Γ_{3w}; the boundaries of the mold exposed to air, Γ_{3a}; and the boundary of the billet exposed to air, Γ_{3b}.

On Γ_{3w}, $T_a=T_w$, where T_w is specified as the temperature of the cooling water; $h=h_w$, where h_w is related to the turbulence Reynolds number R_e and the thermal conductivity of the cooling water λ_w by the Dittus–Boelter equation as

$$h_w = \frac{0.023\lambda_w R_e^{0.8} P_r^{0.4}}{d}, \tag{4}$$

in which P_r is the Prandtl's number, and:

$$R_e = \frac{v_w \cdot d}{\eta_w}, \tag{5}$$

with v_w the velocity of the cooling water and η_w the viscosity of the cooling water (η_w=0.083×10^6 m^2/s at 33°C), and $d = 4\frac{S}{L}$ (m) the equivalent diameter, where S (m^2) and L (m) are the area and the perimeter of the cross-section of the cooling water slot, respectively.

On Γ_{3a}, $T_a=T_{air}$, where T_{air} is the temperature of the surrounding air; and $h=h_{air}$. In the simulation, both T_{air} and h_{air} are treated as constants.

On Γ_{3b}, $T_a=T_{am}$, where T_{am} is the temperature of the surrounding air, and $h=h_{am}$. Both T_{am} and h_{am} are also treated as constants.

The temperature of the input molten steel is about 1,530°C, which is used as the initial volumetric temperature condition. The boundary conditions on the planes of symmetry of the system (Fig. 2) are prescribed as:

$$k\frac{\partial T}{\partial x} = 0 \ (x - y \text{ plane of symmetry}) \tag{6}$$

In a continuous casting process, the contracting solid steel shell surface and the mold surface are separated by a very narrow gap. The contact thermal property of the gap, i.e., the gap conductance, should be introduced. In general, it can be specified as [17]:

$$k_g = k\left(\overline{T}, d, p, \left|\overline{\dot{m}}\right|\right), \tag{7}$$

where $\overline{T} = \frac{1}{2}(T_s + T_m)$ is the average of the temperatures at the surface of the solid shell of the billet T_s and that of the mold T_m, d is the clearance, p is the contact pressure transmitted across the interface, and $\left|\overline{\dot{m}}\right| = \frac{1}{2}\left(\left|\dot{m}\right|_s + \left|\dot{m}\right|_m\right)$ is the average of the magnitudes of the mass flow rates per unit area of the contacting surface.

5 Results and discussion

The distributions of the transient temperature and the deformation in the mold and their variations during casting processes are computed with the commercially available FE code ABAQUS/Standard. The cross-sectional area of the casting billet is 170×1,400 mm, the moving velocity of the billet is 1.2 m/min, and the computation time span is 60 s. Half of the mold–billet system, shown in Fig. 2, is used for the coupled thermal–mechanical analysis. Elements of type C3D8T (an eight-node thermally coupled brick) are adopted in the computation. Before the billet enters the mold, the interfaces between the billet and the mold are assumed to be adiabatic, because the inner surface of the mold over the meniscus does not make contact with the molten steel.

Figure 5 shows the variation of the temperature at a node on the billet surface, which contacts the mold and moves downward against the mold: This signifies the solidification process of the billet. It can be seen in Fig. 5 that for the first 20 s, the temperature of the billet falls gradually from the initial temperature of 1,530°C to a little below the liquidus temperature, the temperature decreasing relatively slowly because of the additional heat (latent heat) released during phase change. When the temperature falls below the solidus temperature (1,490°C), latent heat is no longer released, and the temperature then decreasing sharply. The node leaves the mold at about 42 s. The temperature will remain at about 1,130°C thereafter without considering the air-mist spray cooling in the following cooling stage.

The longitudinal distribution of the temperature at the inner surface of mold at the end of the computation is shown in Fig. 6. It can be seen that both the previous approach with empirical formulae (PA) [11] and the coupled thermal–mechanical analysis for the mold–billet

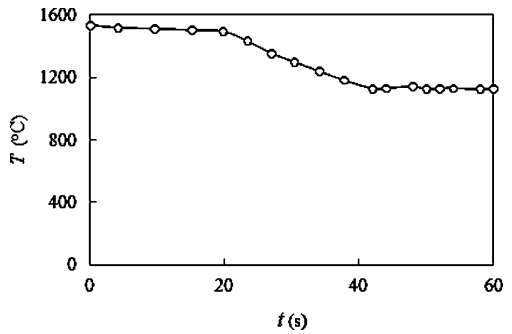

Fig. 5 The variation of the temperature of a node of the billet

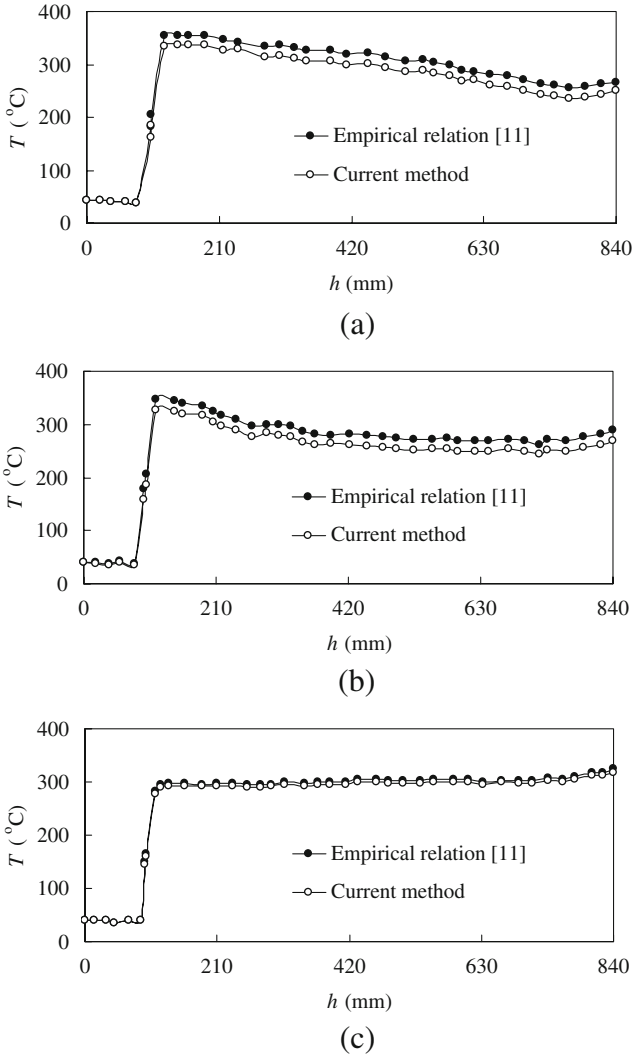

Fig. 6 Longitudinal distribution of temperature at the inner surface of mold at the end of the computation. **a** Main plate (convex), **b** main plate (concave), **c** side plate

system (current method, CM) give the similar distributions of the temperature. It can be seen in Fig. 6a, b that the maximum temperature occurs at the inner surface of the mold. At the inner surface of the main plates, the temperature increases sharply from about 50°C to the peak value, then decreases gradually with the increase of h (where h is the distance from the top surface of the mold, Fig. 2). It is noted that the meniscus is located at h= 100 m and that the molten steel does not contact directly with the inner surface of the mold if h<100 mm. The distribution of temperature in the side plate is shown in Fig. 6c, from which it can be seen that the temperature is at a low level and distributes quite uniformly in the longitudinal direction.

The transverse distributions of the temperature and displacement at the inner surface of mold at h=420 mm are shown in Figs. 7 and 8, respectively (where A is the distance from the plane of symmetry and B is the distance from the surface contacting the inner surface of the main plate [convex], Fig. 2). It can be seen that the temperature distributes quite uniformly, and the temperature distribution obtained using CM is similar to that obtained using PA.

It can be seen in Figs. 7 and 8 that although the results with CM are similar to the that with PA, the average temperature in the main plates obtained with CM is about 20°C lower than that obtained with PA, and the average temperature in the side plate obtained with CM is about 10°C higher than that obtained with PA. This difference should be attributed to the different simplification of the boundary conditions. For PA, the interaction between the billet and the mold is replaced with the empirical relationships, while for CM, the whole mold–billet system is

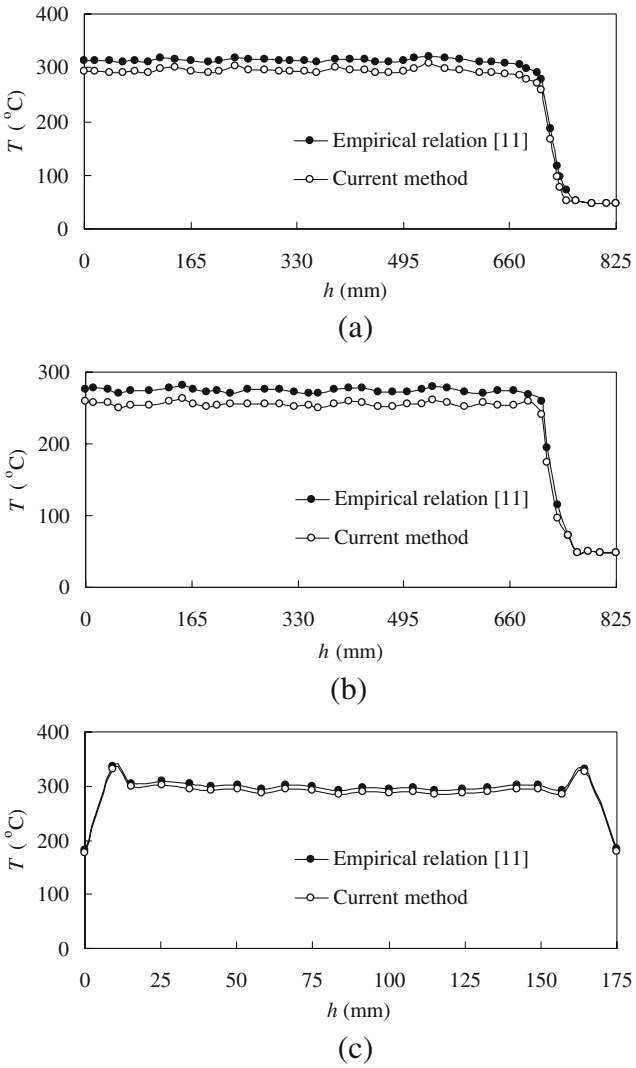

Fig. 7 Transverse distribution of temperature at the inner face of the mold at the end of the computation. **a** Main plate (convex), **b** main plate (concave), **c** Side plate

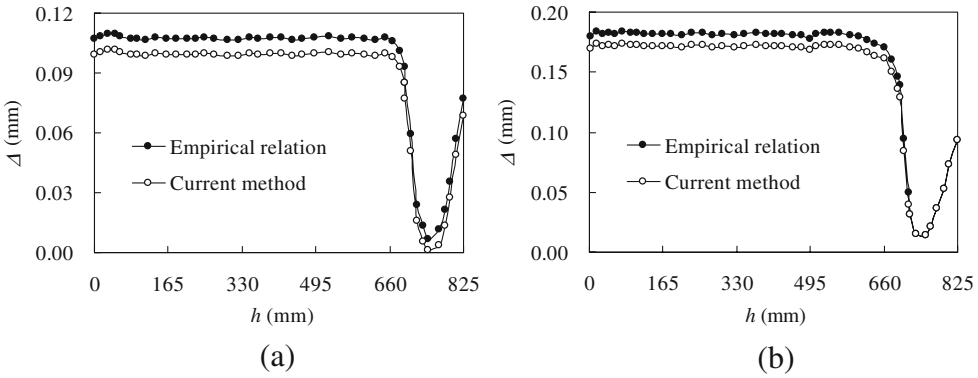

Fig. 8 Transverse distribution of displacement at the inner face of the mold at the end of the computation. **a** Main plate (convex), **b** Main plate (concave)

adopted, and the interaction can be taken into account automatically during the analysis. Other influencing factors, such as radiation from the molten steel and air gap between the contracted billet and the mold, can also be taken into account if the corresponding parameters are provided.

During the analysis, the outer surface of the mold is fixed in the outward normal direction. Figure 8 indicates that at the inner face of the mold the displacement obtained with CM is smaller than that with PA. For PA, the deformation is caused by thermal expansion, and it is free at the inner surface of the mold. However, the displacement with CM includes two parts; besides thermal expansion, the interfacial pressure from the deformed billet also makes contribution, although the direction is opposite. Comparison shows that PA overestimates the displacement, because it ignores the mechanical interaction between the mold and the billet.

The distributions of the temperature in the different cross-sections of the billet are shown in Fig. 9, where it can be seen that the thickness of the solidified shell in a cross-section increases as it moves downward. The thickness of the solidified shell seems to be sufficiently large to hold the remaining molten steel when it moves to the exit of the mold (840 mm below the top surface of the mold).

The longitudinal distribution of Mises stress at the inner surface of the mold at the end of the computation is shown in Fig. 10. It can be seen that when $h>100$ mm, the Mises stress in the coating layer is almost uniform. At the surface of the copper plate, the Mises stress increases slightly after $h>100$ mm. Compared with the material properties given in Fig. 3 and Tables 3 and 4, it can be seen that at the inner surface of the mold, both the coating material and the copper plate are in the yield state. The uniform distribution of Mises stress in the coating material can be attributed to

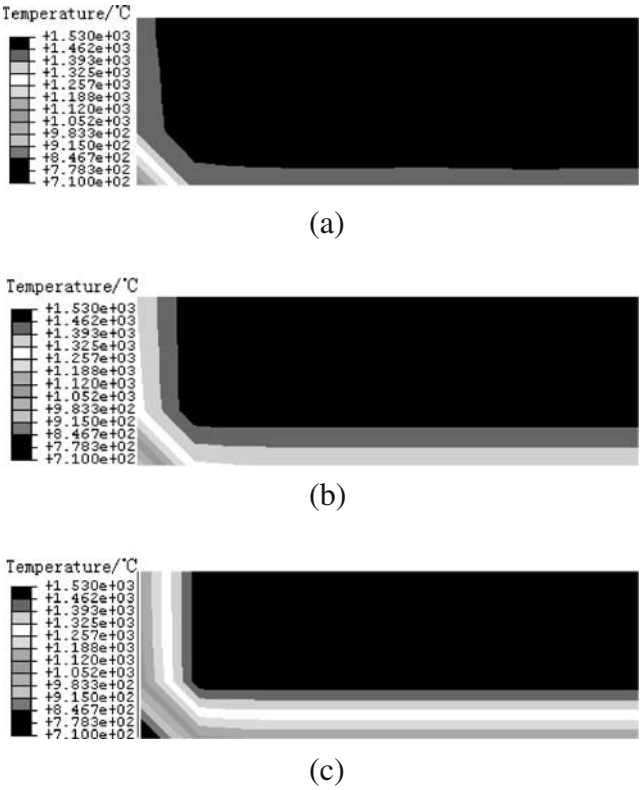

Fig. 9 Distribution of temperature at the cross section of the billet at the end of the computation. (**a**) 300 mm below the top surface of the mold, (**b**) 600 mm below the top surface of the mold, (**c**) 840 mm below the top surface of the mold

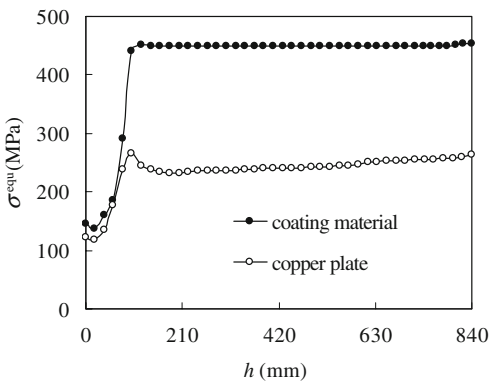

Fig. 10 Longitudinal distribution of the Mises stress at the inner surface of mold at the end of the computation

the assumption that its yield stress is independent of temperature, while the slight increase in the Mises stress in the copper plate with the increase of h can be attributed to the decrease in the temperature with the increase of h and the dependence of the yield stress of the material on temperature (Fig. 3). However, it can be seen in Figs. 7 and 8 that the temperature does not exceed the softening temperature of the copper (500°C), so that the mold will, therefore, have sufficient strength during the continuous casting process. The state of stress at the inner surface of the mold is significant with respect to the estimation of wear, failure, and life of the mold, but it cannot be provided by PA because the mechanical interaction between the mold and billet is ignored.

6 Conclusions

The coupled thermal–mechanical behavior of a mold–billet system during continuous casting is analyzed, in which both three-dimensional transient heat transfer and the thermal–mechanical interaction between the moving billet and the mold are taken into account. Compared with the results obtained previously, the following conclusions can be drawn:

1. The distributions of the temperature and the displacement in the mold obtained are qualitatively and quantitatively agreeable with those obtained previously by making use of the empirical formulae of the heat flux identified with experiment, which demonstrates, indirectly, the validity of the proposed approach.
2. The coupled thermal–mechanical analysis of a mold–billet system can take into account both thermal and mechanical interaction between the mold and the billet, in which only thermal and mechanical properties of the interface are employed, instead of using additional empirical formulae of the heat flux. The latter normally needs to be identified with support of complex experimentation.
3. The adopted approach can provide detailed information of the thermal and mechanical responses, which is much needed for an accurate assessment of the capability and failure of the mold.
4. The adopted approach can avoid possible inconsistency and the corresponding complexity and difficulty caused by splitting the system into two individual parts. Thus, the adopted approach should be of more generality and convenience in application.
5. Other influencing factors related to the interaction between the mold and the billet, such as radiation from the molten steel and the air gap between the contracting billet and the mold, etc, can also be taken into account without difficulty, if the corresponding parameters are provided.

Acknowledgement The authors gratefully acknowledge the financial support to this work from the Natural Science Foundation of China (10472135) and the collaboration between the University of Strathclyde, UK, and Chongqing University, China.

References

1. Huespe AE, Cardona A, Fachinotti V (2000) Thermal–mechanical model of a continuous casting process. Comput Methods Appl Mech Eng 182:439–455 doi:10.1016/S0045-7825(99)00203-0
2. Janik M, Dyja H, Berski S, Banaszek G (2004) Two-dimensional thermal–mechanical analysis of continuous casting process. J Mater Process Technol 153–154:578–582 doi:10.1016/j.jmatprotec.2004.04.129
3. Janik M, Dyja H (2004) Modelling of three-dimensional temperature field inside the mould during continuous casting of steel. J Mater Process Technol 157–158:177–182
4. Santos CA, Spim JA, Garcia A (2003) Mathematical modeling and optimization strategies (genetic algorithm and knowledge base) applied to the continuous casting of steel. Eng Appl Artif Intell 16:511–527 doi:10.1016/S0952-1976(03)00072-1
5. Fic A, Nowak AJ, Bialecki R (2000) Heat transfer analysis of the continuous casting process by the front tracking BEM. Eng Anal Bound Elem 24:215–223 doi:10.1016/S0955-7997(00)00004-7
6. Louhenkilpi S, Makinen M, Vapalahti S, Raisanen T, Laine J (2005) 3D steady state and transient simulation tools for heat transfer and solidification in continuous casting. Mater Sci Eng A 413–414:135–138
7. Zheng XS, Sha MH, Jin JZ (2006) Experimental research and numerical simulation of mold temperature field in continuous casting of steel. Acta Metall Sin (Engl Lett) 19:176–182
8. Tieu AK, Kim IS (1997) Simulation of the continuous casting process by a mathematical model. Int J Mech Sci 39:185–192 doi:10.1016/0020-7403(96)00052-5
9. Wobker H-G, Hugenschutt G, Kolbeck D (2003) Use of FEM simulation to optimize continuous casting moulds. Iron Steel 38:55–58 (in Chinese)
10. Engang W, Zhekun Y, Haigeng C (1996) A study on finite element numerical simulation of the solidification heat transfer of continuous casting slab. Steelmaking 8:30–35 (in Chinese)
11. Peng X, Zhou J, Qin Y (2005) Improvement of the temperature distribution in continuous casting moulds through the rearrangement of the cooling water slots. J Mater Process Technol 167:508–514
12. Wang E, He J (2001) Finite elemet simulation on thermal-mechanical behavior of steel billet in continuous casting mold. Sci Technol Adv Mater 2:257–263
13. Bo Y, Guanghua W, Xiaomin Z (2001) Coupled solidification process of continuous casting slab in mold. Eng Mech 18:110–118 (in Chinese)
14. Lixin C, Jiaquan Z, Suqiong C (2003) Research on solidification of contiuous casting slab in mould. Steelmaking 19:22–25, 30 (in Chinese)
15. Jiongming Z, Li Z, Huitao Y, Xinhua W (2004) Numerical simulation of liquid steel solidification in slab molds. J Univ Sci Technol Beijing 26:130–134 (in Chinese)
16. ABAQUS. Heat transfer. ABAQUS theory manual, 2.11
17. ABAQUS Thermal contact properties. ABAQUS analysis user's manual, 22.2.1